Key Points:
- Part of the deep western boundary current flowing northward along the Tonga Kermadec Ridge is redirected southward between 1,500 and 4,800 m
- Seasonal fluctuations in the upper 2,000 m of the Southwest Pacific Basin are continued into the abyssal ocean with decreasing amplitude
- Deep Argo provides estimates of the deep-ocean circulation complementary to repeat hydrography and moored observations

Correspondence to:
N. V. Zilberman,
nzilberman@ucsd.edu

Deep-Ocean Circulation in the Southwest Pacific Ocean Interior: Estimates of the Mean Flow and Variability Using Deep Argo Data

N. V. Zilberman[1] (iD), **D. H. Roemmich[1]** (iD), **and J. Gilson[1]** (iD)

[1]Scripps Institution of Oceanography, University of California San Diego, La Jolla, CA, USA

Abstract The spatial structure and time variability of the global deep-ocean circulation are poorly understood due to limited sampling below 2,000-m depth. A Deep Argo array deployed in 2016 has significantly increased oceanic measurements from the ocean surface to near the sea floor in the Southwest Pacific Basin interior. Deep Argo profiles collected between 2016 and 2019 show that 4.3–4.7 Sv between 1,500 and 4,800 m, relative to 4,800 m, of the Deep Western Boundary Current flowing along the Tonga Kermadec Ridge is redirected southward over the abyssal plain between the Tonga Kermadec Ridge and the East Pacific Rise. The southward recirculation of the Deep Western Boundary Current exhibits seasonality that may be influenced by Ekman pumping.

Plain Language Summary Observations of the deep-ocean circulation are important for understanding long-term changes in fundamental ocean properties, including temperature and salinity. A newly developed technology, Deep Argo profiling floats, has been deployed in the Southwest Pacific Basin to increase oceanic sampling from the ocean surface to the sea floor. Using this new data set, the circulation in the abyssal Southwest Pacific Basin is mapped outside the Deep Western Boundary Current. Our study shows that part of the deep current flowing northward along the 2,000-km long Tonga Kermadec trench, between the northern tip of New Zealand and the Samoan islands, is redirected southward in the basin interior between 1,500–4,800 m depth. The southward deep return flow may be influenced by the wind-forcing on the sea surface, whose effects are seen to penetrate into the deep-ocean.

1. Introduction

The deep-ocean circulation is closely linked to the transport of heat and freshwater between ocean basins and to air-sea exchanges at high latitude (Purkey et al., 2018). Uncertainties in the strength and rate of the deep-ocean overturning limit the ability of ocean-climate models to accurately predict long-term changes in ocean warming and freshening (Lee et al., 2019). The present work provides new results on the spatial structure of the mean and the seasonal variability of the large-scale deep-ocean circulation in the Southwest Pacific Basin, based on the Deep Argo data set.

Argo is the dominant source of in situ observations of subsurface ocean properties used in ocean forecasting, coupled ocean-climate models, and ocean reanalysis (Roemmich et al., 2015). Below 2,000 m, the maximum depth of Core Argo floats, elements of the deep-ocean observing system consist of repeat hydrographic lines and ocean moorings (Send et al., 2010; Talley et al., 2016). Repeat hydrographic lines provide highly accurate physical and biogeochemical full-depth observations, but the sampling frequency of 5 to 10 years and the large spatial separation between repeat lines leave high uncertainty in estimates of the time-mean spatial structure of ocean properties and circulation (Wunsch, 2007). Deep-ocean moorings resolve fluctuations over a broad range of time scales, but these single point time series stations are limited in their areal coverage and often not maintained for more than 1 to 2 years (Voet et al., 2015, 2016; Whitworth et al., 1999). The deep-ocean is greatly under-sampled compared to the upper ocean (The National Academies, 2017). Over 2 million temperature-salinity profiles have been collected globally in the upper 2,000 m from Argo in the past 20 years, compared to 140,000 profiles below 2,000 m from all historical non-Argo data (Boyer et al., 2013).

Deep Argo is a new Argo Program enhancement, aimed to extend Argo sampling to the sea floor (Jayne et al., 2017). Regional Deep Argo pilot arrays have been implemented to establish the reliability and technical performance of Deep Argo floats and to determine the accuracy and stability of Deep

Argo CTD sensors (Zilberman, 2017). The Southwest Pacific Basin has the densest coverage among the Deep Argo pilot arrays.

The global circulation of dense water masses generated at high latitude is referred to in the literature as the lower cell of the meridional overturning circulation (MOC, Marshall & Speer, 2012). In the Southwest Pacific Basin, the lower cell includes a deep western boundary current (DWBC) that extends below 1,500-m depth to the bottom, flowing northward along the eastern flank of the Tonga Kermadec Ridge (TKR, Whitworth et al., 1999). Upper waters of the DWBC mix with surrounding waters and upwell into lighter waters that return southward (Talley, 2013). According to the circulation scheme of Reid (1986 and 1997), some of the DWBC between 2,000 and 4,000 m turns southeastward around the western side of an anticyclonic gyre located over the abyssal plains between the TKR and the East Pacific Rise (EPR). It then veers northwestward around the eastern side of the gyre, along the western flank of the EPR. Results from Wijffels et al. (2001) show no evident signature of anticyclonic circulation at 32°S, but a broad southward flow is seen below 1,500 m, over the abyssal plain between the DWBC region and the western flank of the EPR. A clear relationship between the DWBC along the TKR and the deep southward flow over the abyssal plain has not been established. The DWBC transport at 32°S shows strong oscillations that may be related to Rossby waves reflected eastward at the TKR (Moore & Wilkin, 1998; Whitworth et al., 1999). The interannual variability of the deep-ocean circulation east of the DWBC is not understood.

An objective of the present analysis is to demonstrate that a robust estimate of the mean circulation is provided by the regional Deep Argo pilot array, as well as to explore the time variability. It is found that the southward flow in the ocean interior corresponds to recirculation of part of the northward flow of the DWBC along the TKR. Further, seasonal variability in the DWBC recirculation appears related to local Ekman pumping. The data and methods of this analysis are presented in section 2, results follow in section 3, and discussion and conclusion are presented in section 4.

2. Data and Methods

Deep Argo profiles collected from 35 Deep SOLO floats deployed in the Southwest Pacific Basin between 2016 and 2019 are used to compute dynamic height and geostrophic velocity and transport. Deep SOLO floats record temperature-salinity-pressure on descent to profile depth, then ascend to parking depth, typically 500-m above the bottom, drift for 8–13 days, and rise to the surface (Roemmich et al., 2019). The deep drifting depth of these floats, in contrast to the 1,000-m drifting depth of Core Argo floats, is aimed to minimize their drift out of the region. The topography of the Southwest Pacific Basin is characterized by seamounts located along the Louisville Ridge (LR) and on the abyssal plain; the bottom depth varies between >6,000 m in the Tonga Kermadec Trench and 4,500 m within the regional Deep Argo array. To provide maximum spatial coverage, we focus on Deep SOLO data between 0 and 4,800 dbar.

Over 2,200 Deep SOLO profiles are used for this analysis (Figure 1). First, a fresh pressure-dependent bias of about 0.003 PSS-78 at 5,000 dbar is removed by correcting the SBE-61′s conductivity cell compressibility as recommended by Murphy and Martini (2018) and discussed in Zilberman et al. (2019). Then, the accuracy and stability of the Deep Argo salinity measurements are assessed by comparison with recent GO-SHIP repeat hydrography data, including observations along lines P15S, P16, and P06 between 2004 and 2016. GO-SHIP profiles show small spatial variability in salinity (<0.002 PSS-78) on the coldest potential temperature surfaces ($\Theta < 0.8°C$) in the Southwest Pacific Basin. This allows Deep Argo salinity profiles to be validated or adjusted in some cases. For Deep Argo profiles showing salinity difference (with respect to GO-SHIP) greater than 0.002 PSS-78 at 0.74–0.78°C, a depth-independent salinity offset is applied. A few Deep Argo conductivity measurements show slow sensor drift (<0.002 PSS-78 year^{-1}), and for these profiles, salinity values are corrected by removing estimates of a least squares linear fit to salinity drift at 0.74–0.78°C. In any case, the present analysis is focused on dynamic height and geostrophic velocity, which are dominated by temperature variations and for which the small residual salinity errors are not significant.

Time-mean dynamic height fields referenced to 4,800 dbar are computed from Deep Argo temperature and salinity profiles; the inferred dynamic height is then horizontally mapped using a Gaussian fit with isotropic e-folding scale of 6° × 6°. Deep Argo and Core Argo float trajectories are calculated from GPS fixes at the beginning and end of the float′s ~10-min surface time, following Zilberman et al. (2014). Trajectory-based velocities at nominal pressure of 4,800 dbar are calculated from Deep Argo float displacement at parking
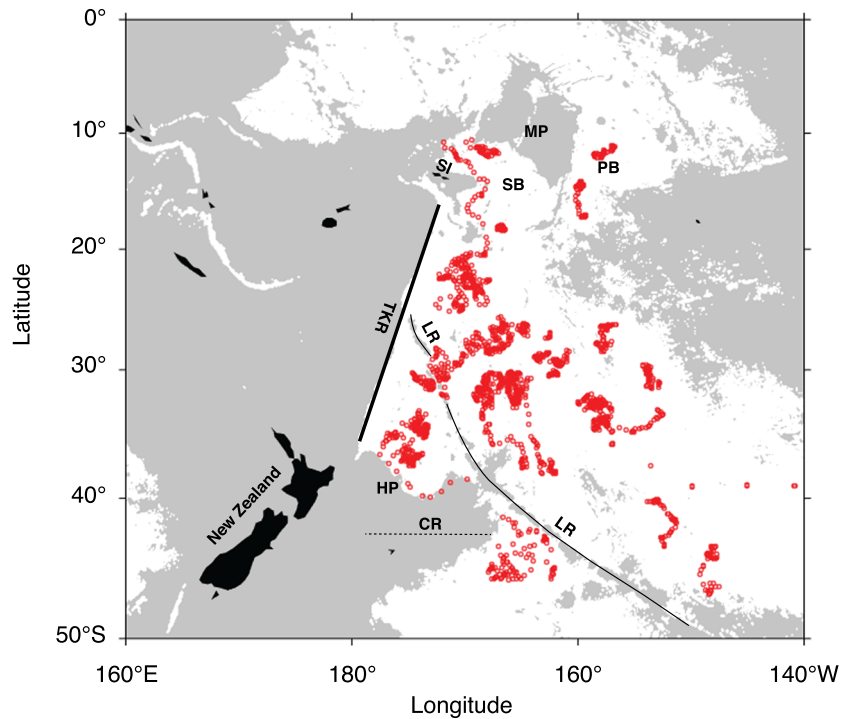
Figure 1. Positions of Deep Argo profiles collected from January 2016 to December 2019 are indicated in squared red symbols. The shaded gray color indicates bottom depth shallower than 4,800-m depth, and the white background color shows regions deeper than 4,800 m. The Samoan Islands (SI), Samoan Basin (SB), Manihiki Plateau (MP), Penrhyn Basin (PB), Louisville Ridge (LR, thin black line), Tonga Kermadec Ridge (TKR, thick black line), Hikurangi Plateau (HP), Chatham Rise (CR, dashed black line), and New Zealand are indicated.

pressures of 4,600–5,000 dbar, and velocities at nominal pressure of 1,000 dbar are calculated from Core Argo float displacement at parking pressures of 800–1,200 dbar. Errors in absolute geostrophic velocities at parking pressure are computed using the standard deviation in trajectory-based velocity and trajectory density per 6° × 6° bin (supporting information Figures S1 and S2). The standard error in Core Argo trajectory-based velocities per 6° × 6° bin is lower than Deep Argo due to the much larger number of Core Argo floats (Figures S1 and S2). For this reason, absolute velocity fields between 0 and 4,800 dbar are computed using Core Argo float trajectory-based velocities at 1,000 dbar combined with 0–4,800 dbar Deep Argo shear profiles. Time-mean absolute height fields at 1,000 dbar are inferred from Core Argo float trajectory-based velocities at 1,000 dbar that are averaged over 6° × 6° bins, using the objective mapping algorithm described in Bretherton et al. (1976) and Gille (2003), and Gaussian decorrelation with isotropic e-folding scale of 6° × 6°. The e-folding scale used in the calculation of absolute dynamic height at 1,000 dbar is chosen for consistency with estimates of dynamic height referenced to 4,800 dbar. The time-mean absolute dynamic height field at 1,000 dbar is then horizontally mapped using a Gaussian fit with isotropic e-folding scale of 12° × 12° to filter out the noise generated by mesoscale features. Here, time-mean estimates of absolute dynamic height are calculated from the dynamic height relative to 4,800 dbar by substracting the height at 1,000 dbar relative to 4,800 dbar and adding the absolute height at 1,000 dbar to each pressure level as

$$\delta_a(p) = \delta(p/4800) - \delta(1000/4800) + \delta_a(1000) \tag{1}$$

where p is pressure, $\delta(p/4,800)$ is dynamic height referenced to 4,800 dbar, $\delta(1,000/4,800)$ is dynamic height at 1,000 dbar referenced to 4,800 dbar, and $\delta_a(1,000)$ is absolute height at 1,000 dbar. Time-mean transport function (TF, Whitworth, 1980) estimates presented in section 3.1 correspond to the depth-integrated time-mean dynamic height. The geostrophic transport normal to and between any pair of points is equal to the difference in TF scaled by the Coriolis parameter. Hence, for a TF difference of 1 m³ s⁻² at 30°S, the corresponding transport is 1.4×10^4 m³ s⁻¹ (Figure 2). Time-mean absolute
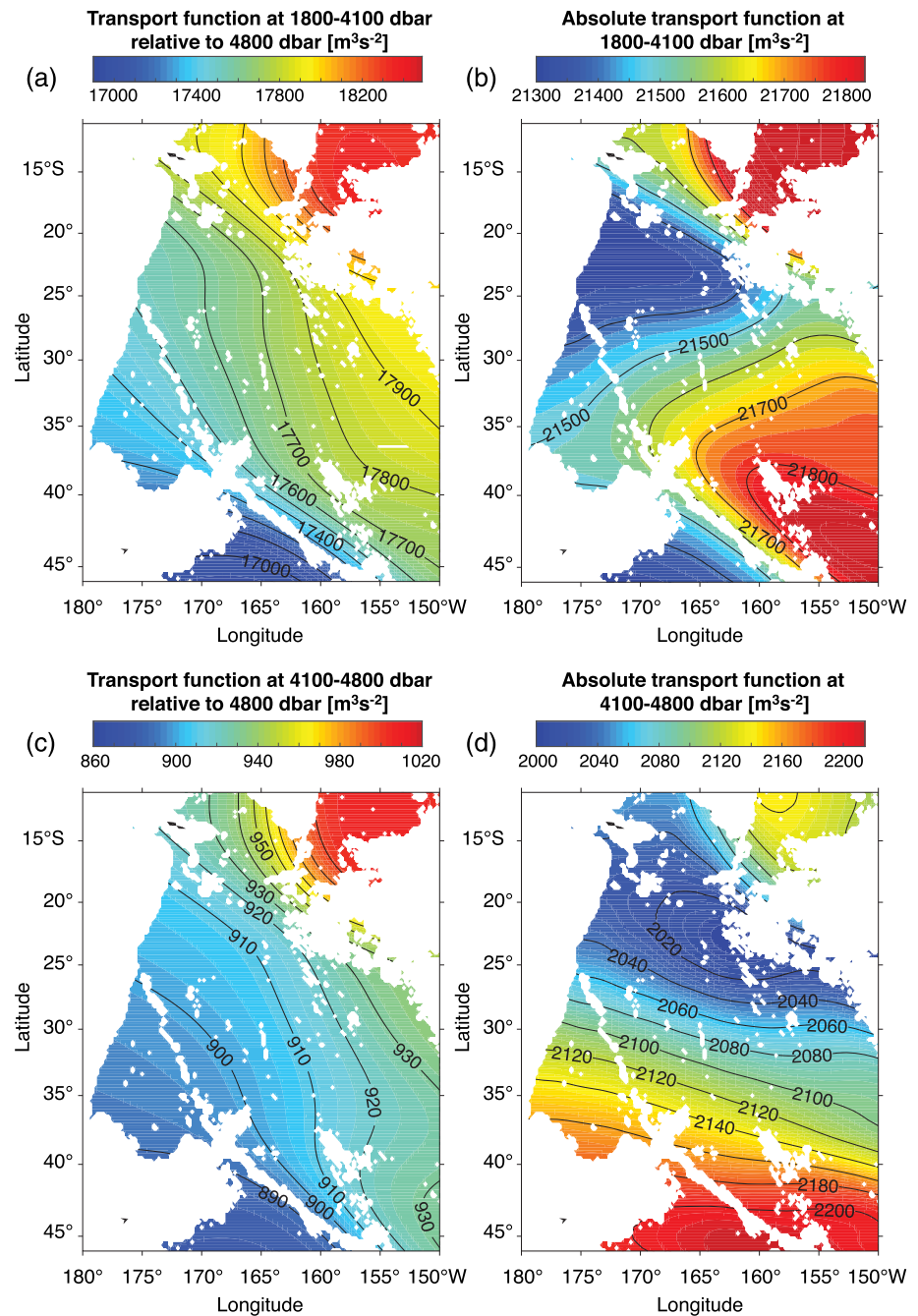
Figure 2. (a) Transport function using a reference level of no motion at 4,800 dbar; (b) absolute transport function integrated between 1,800 and 4,100 dbar for 2016–2019; (c) transport function using a reference level of no motion at 4,800 dbar, and (d) absolute transport function integrated between 4,100 and 4,800 dbar for 2016–2019. The white background color indicates regions shallower than 4,800 m.

geostrophic velocity estimates are inferred from the sum of geostrophic velocity referenced to 4,800 dbar, calculated from temperature and salinity profiles through the thermal wind relationship, and trajectory-based velocity at 1,000 dbar (Gill, 1982, pp. 215–216). Errors in velocity relative to 4,800 dbar are computed based on standard deviation in dynamic height and profile density per 6° × 6° bin. Absolute transport estimates presented in section 3.1 include adjustment for shear-induced error that results from the vertical shear in horizontal velocity during the float ascent and descent between the ocean surface and the 4,800-dbar parking depth. Here, shear-induced error is estimated from

geostrophic shear between 0 and 4,800 dbar and considering that the float spends 1.5 days, 15% of the cycle time, during ascent and descent to parking depth. Estimates of absolute velocity fields between 0 and 2,000 dbar, computed using Core Argo profiles and Core Argo trajectory-based velocities at 1,000 dbar, are presented for comparison. Errors in velocity relative to 2,000 dbar are computed based on standard deviation in dynamic height and profile density per $6° \times 6°$ bin.

3. Results

3.1. Time-Mean Ocean Circulation

Maps of the TF based on Deep Argo profiles and Core Argo trajectories are used to describe the spatial structure of the deep-ocean circulation in the Southwest Pacific Basin. It should be kept in mind that much of the northward transport in the Southwest Pacific Basin is in the DWBC, which has not yet accumulated enough Deep Argo profiles for accurate representation. The analysis presented here is limited to the broader flows in the basin interior.

The 2016–2019 mean estimates of the TF relative to 4,800 dbar and absolute TF are calculated for a deep layer of 1,800–4,100 dbar, and an abyssal layer of 4,100–4,800 dbar (Figure 2). The separation between these two layers is made because the absolute meridional flow reverses direction around 4,100 dbar, as shown in Figure 3. The standard errors ($<7.5 \text{ m}^3 \text{ s}^{-2}$) in TF are relatively small (Figures S3a and S3b). The geostrophic flow in the Southern Hemisphere is oriented anticlockwise around high TF centers. Strong zonal gradients in TF are indicative of intensified meridional transport. Between 46° and 11°S, TF estimates referenced to 4,800 dbar show a dominant southeastward flow in the deep layer, out of the DWBC that flows along the TKR, and across the abyssal plain of the Southwest Pacific Basin (Figure 2a). These results are qualitatively in agreement with the circulation described by Reid (1986). TF estimates in the absolute calculation show a southward flow in and out of the DWBC region (Figure 2b). In the abyssal layer, the TF referenced to 4,800 dbar indicates modest southward flow (Figure 2c). In contrast, absolute transport fields show a broad northwestward flow between 43°–23°S in the opposite direction to the TF estimates referenced to 4,800 dbar (Figures 2c and 2d). The deep flow estimates for 2016–2019 seem to be robust, as reducing the averaging period to 2017–2018 has a limited impact on the magnitude of the transport (Figures 2 and S4).

Figure 3 shows the depth distribution of the time-mean meridional component of geostrophic velocities at 31°S and 37°S, between 172° and 160°W. These latitudes were chosen because they have densest Deep Argo float sampling (>40 profiles) per $6° \times 6°$ bin (Figure S1a). Here, southward flow is indicated by negative velocity values. At 31°S, geostrophic velocities relative to 4,800 dbar (red line) are oriented southward between 1,500 and 4,800 dbar, and results show strongest velocity values ($<-0.1 \text{ cm s}^{-1}$) at the core of the southward flow between 2,000–4,000 dbar (Figure 3a). Characteristics of the deep velocity field at 37°S are consistent with 31°S estimates, including southward flow between 1,500 and 4,800 dbar, and strongest southward velocities between 2,000 and 4,000 dbar (Figures 3a and 3b). Taken together, Figures 2 and 3 indicate the relationship of the absolute to the relative flow in both their spatial patterns and magnitudes. Vertical shear in horizontal velocity between 4,800 and 5,200 dbar (not shown) indicates that absolute northward velocities increase below 4,800 dbar. The Deep Argo-based velocity field described here is consistent with the inverse solution by Wijffels et al. (2001), although the core of the deep southward flow in the inverse solution is located about 10° east of the Deep Argo estimates. The velocity estimates in this study are consistent with long-term circulations that are calculated using the World Ocean Atlas 2018 (WOA18, Figure S5); differences with respect to historical data analyses could be indicative of the historical undersampling or of long time-scale circulation variability.

Figure 3 also shows estimates of absolute geostrophic velocities calculated between 0 and 2,000 dbar using Core Argo profiles and Core trajectory data (blue line), and velocities between 0 and 4,800 dbar using Deep Argo profiles and Core trajectory data (gray line). Absolute velocities using Deep Argo profiles and Core trajectory data indicate a southward flow that lies mostly within 1,800–4,100 dbar, with core centered at 3,000 dbar, in agreement with the referenced calculation. Below 4,100 dbar, the absolute calculation indicates northward velocities of smaller magnitude than in the southward flow above and in opposite direction to the referenced calculation. Absolute geostrophic velocities calculated using Core Argo profiles and Core trajectory data are consistent with estimates using Deep Argo profiles and Core trajectory data. Differences between the two calculations are larger at 37°S than 31°S and are likely due to Deep Argo sampling
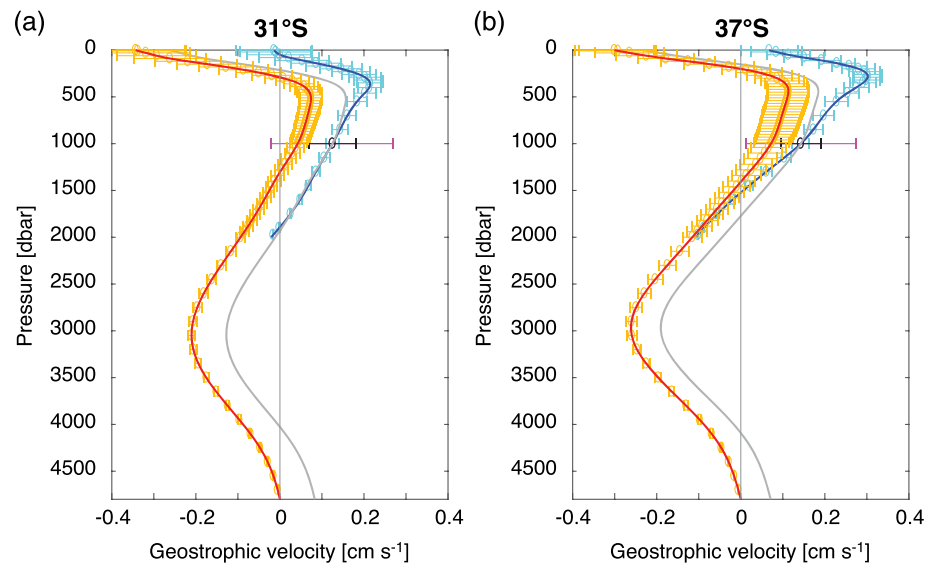
Figure 3. Geostrophic velocity estimates relative to 4,800 dbar computed using Deep Argo profiles (red), absolute geostrophic velocity computed using Deep Argo profiles combined with Core Argo trajectory-based velocities at 1,000 dbar (gray), and absolute geostrophic velocity computed using Core Argo profiles combined with Core Argo trajectory-based velocities at 1,000 dbar (dark blue) at (a) 31°S and (b) 37°S, averaged between 172°W and 160°W. Errors in velocity relative to 4,800 dbar are shown in orange error bars. Errors in velocity relative to 2,000 dbar are shown in light blue error bars. Errors in Core Argo trajectory-based velocities at 1,000 dbar, averaged from 2016 to 2019 are indicated in magenta error bars. These are reduced by 50% if the complete Core Argo data set is used (black error bars).

density being smaller than Core Argo. Velocities at 1,000 dbar using Core Argo trajectories of 2004–2019 show similar time-averaged values but uncertainties 50% smaller than 2016–2019 (black error bars).

The time-mean estimates of southward meridional transport relative to 4,800 dbar, integrated vertically between 1,500 and 4,800 dbar and zonally between 172 and 160°W, are 4.3 ± 0.3 Sv at 31°S, and 4.7 ± 0.5 Sv at 37°S. For comparison, the time-mean estimates of southward absolute meridional transport between 1,800 and 4,100 dbar, integrated zonally between 172–160°W, are 1.8 ± 3.3 Sv at 31°S, and 2.6 ± 2.8 Sv at 37°S. Errors in the estimates of absolute transport are reduced to 1.6 Sv at 31°S and 1.4 Sv at 37°S when using the 15-year Core Argo trajectories.

Another important aspect of the Argo data set is illustrated in Figure 3, namely, the contrast in error levels between geostrophic shear from Argo profile data and absolute velocity from Argo trajectories. The trajectory-based velocity estimates are noisy, containing aliased tides and inertial motions, and other high frequency fluctuations, as well as errors from displacement on the sea surface or while sinking and rising (Park et al., 2004, 2005). Errors in Core Argo trajectory-based velocities will decrease as the number of active Core Argo floats transmitting via Iridium telecommunication system relative to Service Argos increases. The geostrophic shear estimates are effectively low-pass filtered, unaffected by some of the noise sources, and the resulting smaller error bars for shear are evident in Figure 3. Arguably, this contrast in error levels is well known in the literature of absolute geostrophic circulation (Davis, 1998) but is nonetheless noteworthy in the present analysis. Statistical confidence is considerably greater in estimated shear (Figure 3) and relative transport (Figure 2) than in the absolute velocity estimates. As noted above, the errors in estimates of the time-mean absolute velocity at 1,000 dbar are reduced by 50% if the full Argo time-span is used, in contrast with the 4-year span of Deep Argo in the Southwest Pacific Basin. Results shown here range from marginal to high in statistical confidence, perhaps highlighting again the value of historical analyses of geostrophic shear, while also providing initial estimates of the absolute flow, whose uncertainty will decrease with a lengthening Deep Argo data set.

3.2. Seasonal Variability in the Deep-Ocean

Seasonal changes in the deep Southwest Pacific Basin are studied using monthly means of dynamic height based on time series of at least a year collected from 27 individual Deep SOLO floats. The time series from
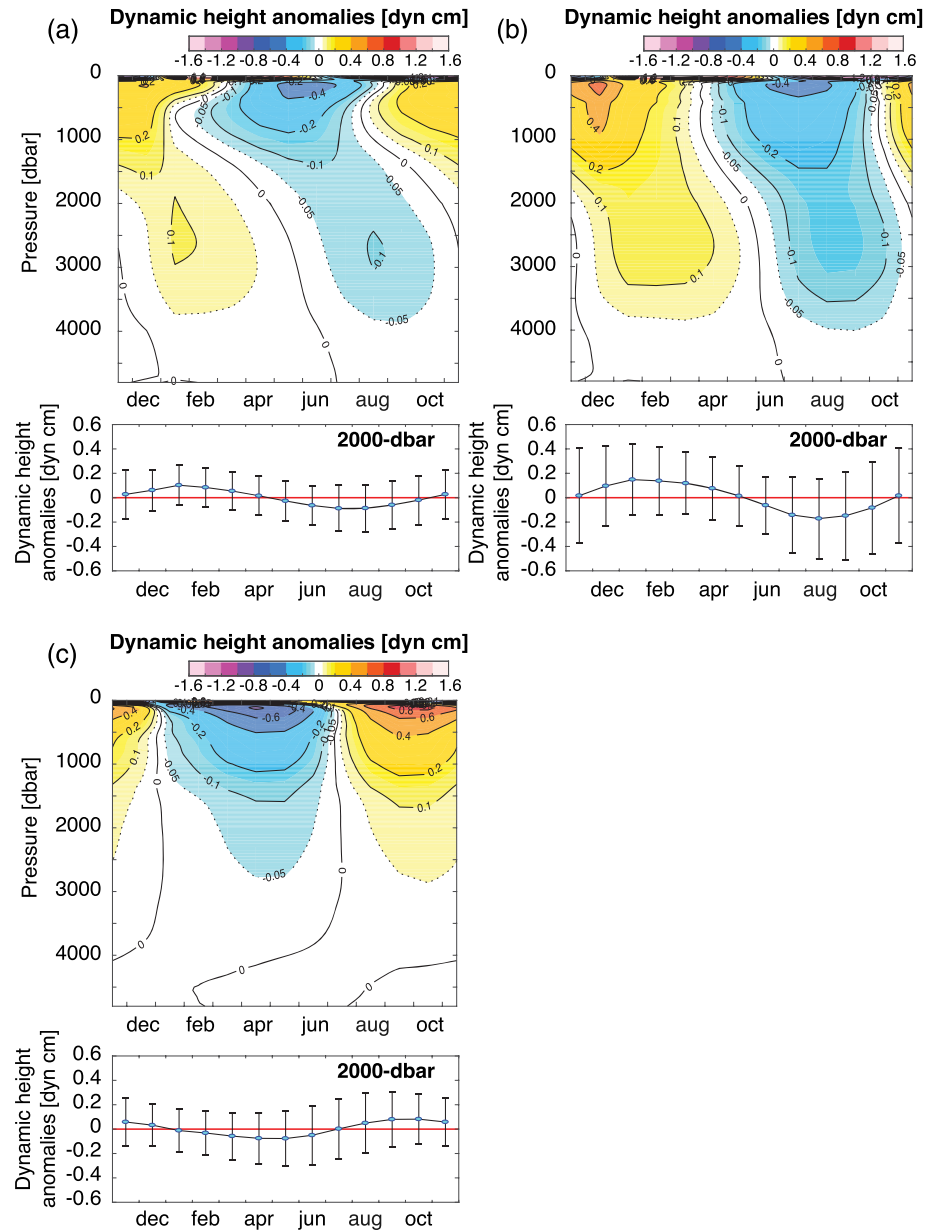
Figure 4. Seasonal variability of dynamic height referenced to 4,800 dbar between 0 and 4,800 dbar and at 2,000 dbar using Deep Argo data of 2016–2019 (a) between 46° and 11°S, (b) between 46° and 32°S, and (c) between 32° and 15°S. Standard error in monthly means of dynamic height at 2,000 dbar are shown in black error bars.

each float are smoothed using a 3-month triangle filter to reduce noise generated by mesoscale features and partitioned into 1-year segments. Dynamic height anomalies averaged for all 1-year segments between 46°– 11°S show apparent seasonal variations characterized by higher values in the hemispheric summer than winter, with this signal decreasing with depth (Figure 4a). Monthly means of Ekman pumping anomalies are calculated between 2016 and 2019 for consistency with the Deep Argo data set, using reanalysis fields from the European Centre for Medium-Range Weather Forecasts Re-Analysis archive (Berrisford et al., 2009; http://data-por-tal.ecmwf.int/). Ekman pumping anomalies in the Southwest Pacific Basin show zonally averaged seasonal anomalies during hemispheric summer that are negative (downward) at mid-latitudes (between 46° and 32°S) and reverse sign in the tropics (between 32° and 15°S, Figure S6). Seasonal variations of Deep Argo dynamic height at mid-latitudes show an apparent 5-month lag with estimates in the tropics, in qualitative agreement with local Ekman pumping (Figures 4b, 4c, and S6). The

annual cycle in dynamic height is likely reduced near 32°S, where the local Ekman pumping reverses sign. The phase difference between the upper layer at 0–3,000 m and the deep layer below 3,000 m suggests that additional processes including horizontal advection from mesoscale eddies and Rossby wave propagation, and vertical advection from diapycnal mixing may contribute to the seasonal changes in dynamic height. Monthly mean estimates between 46°–11°S are based on a limited data set that includes 21 segments between 46° and 32°S, 21 between 32° and 15°S, and 5 between 15° and 11°S. Standard errors in dynamic height, based on standard deviations of the monthly estimates and number of observation per month, indicate a weakly significant signal at 2,000 dbar (Figures 4a–4c). Uncertainties in the seasonal variability of the deep-ocean circulation in the Southwest Pacific Basin will decrease as Deep Argo sampling density increases. An in-depth analysis of the effect of Ekman pumping on the meridional transport is beyond the scope of this work.

4. Discussion and Conclusion

The spatial structure, depth dependence, and time variability of the deep transport in the Southwest Pacific Basin were investigated using Deep Argo profiles and trajectory data collected from a regional Deep Argo array between January 2016 and December 2019. An important aspect of the pilot phase of Deep Argo is to explore and demonstrate the scientific value of the Deep Argo data set, and its complementary relationship to other observing systems including repeat hydrographic lines and deep-ocean moorings. The two main results of this work are the following.

First, a deep southward mean flow in the 1,500–4,800 dbar layer is observed between 46° and 11°S over the abyssal plain between the TKR and the EPR. The maximum in southward flow is found at 3,000 dbar at both 31°S and 37°S. It is similar in absolute transport using trajectory data and as relative transport using a deep reference level of 4,800 dbar. Our analysis shows that the deep water pathway corresponds to a southward recirculation of a portion of the DWBC that flows northward along the eastern flank of the TKR. However, the 3,000-dbar maximum in the southward interior velocity is shallower than the 5,000-dbar northward velocity maximum in the DWBC (Whitworth et al., 1999) and shallower than the deep water masses—North Atlantic Deep Water and Antarctic Bottom Water. Thus it is primarily the upper portion of the DWBC that is being recirculated in the interior.

The newly established relationship between the DWBC and the deep flow over the abyssal basin improves our understanding of deep transport in the Pacific Ocean. The Samoan Passage and adjacent region is the main gateway linking the northward deep water flow in the South Pacific with that in the North Pacific Ocean. Previous moored observations indicated that the deep transport in the DWBC at 32°S is about 16.0 ± 11.9 Sv, while the transport summed in the Samoan Passage and nearby pathways around 10°S is about 11 Sv (Roemmich et al., 1996; Voet et al., 2015; Whitworth et al., 1999). In order for consistency in the net transport estimates at 10°S and 32°S, about 5 Sv of the DWBC flow must recirculate southward. Results from Wijffels et al. (2001) show a southward transport of 8–10 Sv below 1,200 m, between the TKR and the EPR. Qualitative results from Reid (1986 and 1997), indicate no evident southward recirculation of the DWBC. Deep Argo results presented here indicate 4.3 Sv of the northward flow in the DWBC is redirected southward across 31°S between 172°W and 160°W. With additional southward flow west of 172°W and east of 160°W, the interior circulation described here is consistent with the estimated 5 Sv transport reduction in the DWBC based on moored array observations. This consistency between independent observations demonstrates Deep Argo's ability to provide a robust estimate of the mean circulation and transport, and Deep Argo's value, complementary to existing elements of the deep-ocean observing system, to study the net transport of DWBC and recirculation.

It is also seen that the deep-ocean wind-driven flow in the Southwest Pacific Ocean interior varies modestly at the seasonal time scale. According to Giglio et al. (2013) and Giglio (2014), the seasonal variability of isopycnal displacement in the upper ocean is related to Ekman pumping. Our measurements suggest that the seasonal displacements extend downward, perhaps to 3,000 or 4,000 dbar, and hence that the southward recirculation of the DWBC may be influenced by seasonal Ekman pumping. Results suggest that seasonal anomalies in the deep transport are reduced near 32°S, where there is weaker zonally averaged seasonal variation in Ekman pumping. This finding is consistent with earlier DWBC transport estimates from moored data, showing no apparent annual cycle at 32°S (Whitworth et al., 1999). In addition to providing

broad-scale coverage complementary to ocean stations and hydrographic sections, while repeat hydrography supplies high-accuracy reference data for Deep Argo quality control, Deep Argo's systematic and regular sampling will be useful to reduce sampling error in deep-ocean circulation estimates and to eliminate seasonal bias in ship-based deep-ocean observations.

Data Availability Statement

The Deep Argo data used here (http://doi.org/10.17882/42182) were collected and made freely available by the International Argo Program and the national programs that contribute to it.

References

Berrisford, P., Dee, D., Fielding, K., Fuentes, M., Kallberg, P., Kobayashi, S., & Uppala, S. (2009). The ERA-Interim archive, version 1.0, For medium range weather forecasts. Tech.Rep., Eur. Cent. Shinfield Park, Reading, Berkshire, U. K.

Boyer, T. P., Antonov, J. I., Baranova, O. K., Coleman, C., Garcia, H. E., Grodsky, A., et al. (2013). World Ocean database 2013, S. Levitus, Ed., A. Mishonov, technical Ed.; NOAA atlas NESDIS 72, silver spring, MD, 209 pp., http://doi.org/10.7289/V5NZ85MT

Bretherton, F. P., Davis, R. E., & Fandry, C. B. (1976). A technique for objective analysis and design of oceanographic experiments applied to MODE 73. *Deep Sea Research*, 23, 559–582.

Davis, R. E. (1998). Preliminary results from directly measuring middepth circulation in the tropical and South Pacific. *Journal of Geophysical Research*, 103(C11), 24,619–24,639. https://doi.org/10.1029/98JC01913

Giglio, D. (2014). Large-Scale Ocean circulation, dynamics, and air-sea exchanges: Argo observations of the mean and time-varying ocean, UC san Diego, ProQuest ID: Giglio_ucsd_0033D_14485. Merritt ID: Ark:/20775/bb86708034. https://escholarship.org/uc/item/3hx9k3jm

Giglio, D., Roemmich, D., & Cornuelle, B. (2013). Understanding the annual cycle in global steric height. *Geophysical Research Letters*, 40, 4349–4354. https://doi.org/10.1002/grl.50774

Gill, A. E. (1982). *Atmosphere-ocean dynamics*, (p. 662). New York: Academic press.

Gille, S. T. (2003). Float observations of the Southern Ocean part I: Estimating mean fields, bottom velocities, and topographic steering. *Journal of Physical Oceanography*, 33(6), 1167–1181. https://doi.org/10.1175/1520-0485(2003)033<1167:FOOTSO>2.0.CO;2

Jayne, S. R., Roemmich, D. H., Zilberman, N. V., Riser, S. C., Johnson, K. S., Johnson, G. C., & Piotrowicz, S. R. (2017). The Argo program: Present and future. *Oceanography*, 30(2), 18–28. https://doi.org/10.5670/oceanog.2017.213

Lee, S. K., Lumpkin, R., Baringer, M. O., Meinen, C. S., Goes, M., Dong, S., et al. (2019). Global meridional overturning circulation inferred from a data-constrained ocean & sea-ice model. *Geophysical Research Letters*, 46, 1521–1530. https://doi.org/10.1029/2018GL080940

Marshall, J., & Speer, K. (2012). Closure of the meridional overturning circulation through Southern Ocean upwelling. *Nature Geoscience*, 5(3), 171–180. https://doi.org/10.1038/NGEO1391

Moore, M. I., & Wilkin, J. L. (1998). Variability in the South Pacific deep western boundary current from current meter observations and a high-resolution global model. *Journal of Geophysical Research*, 103(C3), 5439–5457. https://doi.org/10.1029/97JC03207

Murphy, D. & Martini, K. (2018). Determination of conductivity cell compressibility for Argo program CTDs and MicroCATs, Poster IS24E-2622, Presented at 2018 Ocean Sciences Meeting, Portland, OR, 12–16 Feb.

Park, J. J., Kim, K., & Crawford, W. R. (2004). Inertial currents estimated from surface trajectories of Argo floats. *Geophysical Research Letters*, 31, L13307. https://doi.org/10.1029/2004GL020191

Park, J. J., Kim, K., King, B., & Riser, S. (2005). An advanced method to estimate deep currents from profiling floats. *Journal of Atmospheric and Oceanic Technology*, 22(8), 1294–1304. https://doi.org/10.1175/JTECH1748.1

Purkey, S. G., Smethie, W. M. Jr., Gebbie, G., Gordon, A. L., Sonnerup, R. E., Warner, M. J., & Bullister, J. L. (2018). A synoptic view of the ventilation and circulation of Antarctic bottom water from chlorofluorocarbons and natural tracers. *Annual Review of Marine Science*, 10(1), 503–527. https://doi.org/10.1146/annurev-marine-121916-063414

Reid, J. (1986). On the total geostrophic circulation of the South Pacific Ocean: Flow patterns, tracers, and transports. *Progress in Oceanography*, 16(1), 1–61. https://doi.org/10.1016/0079-6611(86)90036-4

Reid, J. (1997). On the total geostrophic circulation of the Pacific Ocean: Flow patterns, tracers, and transports. *Progress in Oceanography*, 39(4), 263–352. https://doi.org/10.1016/S0079-6611(97)00012-8

Roemmich, D., Church, J., Gilson, J., Monselesan, D., Sutton, P., & Wijffels, S. (2015). Unabated planetary warming and its ocean structure since 2006. *Nature Climate Change*, 5(3), 240–245. https://doi.org/10.1038/nclimate2513

Roemmich, D., Hautala, S., & Rudnick, D. (1996). Northward abyssal transport through the Samoan passage and adjacent regions. *Journal of Geophysical Research*, 101(C6), 14,039–14,055. https://doi.org/10.1029/96JC00797

Roemmich, D., Sherman, J. T., Davis, R. E., Grindley, K., McClune, M., Parker, C. J., et al. (2019). Deep SOLO: A full-depth profiling float for the Argo program. *Journal of Atmospheric and Oceanic Technology*, 36(10), 1967–1981. https://doi.org/10.1175/jtech-d-19-0066.1

Send, U., Weller, R., Wallace, D., Chavez, F., Lampitt, R., Dickey, T., et al. (2010). In J. Hall, D. E. Harrison, & D. Stammer (Eds.), *"OceanSITES" in Proc. of OceanObs'09: Sustained ocean observations and information for society*, (p. 2), 21-25 September 2009. Venice, Italy: ESA Publication WPP-306. https://doi.org/10.5270/OceanObs09.cwp.79

Talley, L. D. (2013). Closure of the global overturning circulation through the Indian, Pacific, and southern oceans: Schematics and transports. *Oceanography*, 26(1), 80–97. https://doi.org/10.5670/oceanog.2013.07

Talley, L. D., Feely, R. A., Sloyan, B. M., Wanninkhof, R., Baringer, M. O., Bullister, J. L., et al. (2016). Changes in ocean heat, carbon content, and ventilation: A review of the first decade of GO-SHIP global repeat hydrography. *Annual Review of Marine Science*, 8(1), 185–215. https://doi.org/10.1146/annurev-marine-052915-100829

The National Academies of Sciences, Engineering, and Medicine (2017). *Sustaining ocean observations to understand future changes in Earth's climate*. Washington, DC: The National Academies Press. https://doi.org/10.17226/24919

Voet, G., Alford, M. H., Girton, J. B., Carter, G. S., Mickett, J. B., & Klymak, J. M. (2016). Warming and weakening of the abyssal flow through the Samoan passage. *Journal of Physical Oceanography*, 46(8), 2389–2401. https://doi.org/10.1175/JPO-D-16-0063.1

Voet, G., Girton, J. B., Alford, M. H., Carter, G. S., Klymak, J. M., & Mickett, J. B. (2015). Pathways, volume transport, and mixing of abyssal water in the Samoan passage. *Journal of Physical Oceanography*, 45(2), 562–588. https://doi.org/10.1175/JPO-D-14-0096.1

Whitworth, T. (1980). Zonation and geostrophic flow of the Antarctic circumpolar current at Drake Passage. *Deep Sea Research*, *27*(7), 497–507. https://doi.org/10.1016/0198-0149(80)90036-9

Whitworth, T., Warren, B. A., Nowlin, W. D., Rutz, S. B., Pillsbury, R. D., & Moore, M. I. (1999). On the deep western-boundary current in the Southwest Pacific Basin. *Progress in Oceanography*, *43*(1), 1–54. https://doi.org/10.1016/S0079-6611(99)00005-1

Wijffels, S. E., Toole, J. M., & Davis, R. (2001). Revisiting the South Pacific subtropical circulation: A synthesis of World Ocean circulation experiment observations along 32°S. *Journal of Geophysical Research*, *106*(C9), 19,481–19,513. https://doi.org/10.1029/1999JC000118

Wunsch, C. (2007). The past and future ocean circulation from a contemporary perspective. In A. Schmittner, J. Chiang, & S. Hemming (Eds.), *Ocean circulation: Mechanisms and impacts, Geophys. Monogr. Ser.*, Vol. 173, (pp. 53–74). Washington, D. C: AGU.

Zilberman, N. V. (2017). Deep Argo—Sampling the total ocean volume, Bulletin of the American Meteorological Society. *State of the Climate in 2016 report*, *8*(98), 73–74.

Zilberman, N. V., B. King, S. Purkey, V. Thierry, and D. Roemmich (2019). Report on the 2nd Deep Argo Implementation Workshop, Hobart, May 13-15th 2019, https://archimer.ifremer.fr/doc/00507/61873/

Zilberman, N. V., Roemmich, D., & Gille, S. (2014). Meridional volume transport in the South Pacific: Mean and SAM-related variability. *Journal of Geophysical Research*, *119*, 2658–2678. https://doi.org/10.1002/2013JC009688